The Journal of Experimental Biology 201, 3041–3055 (1998)
Printed in Great Britain © The Company of Biologists Limited 1998
JEB1610

MECHANICS OF THE FAST-START: MUSCLE FUNCTION AND THE ROLE OF INTRAMUSCULAR PRESSURE IN THE ESCAPE BEHAVIOR OF *AMIA CALVA* AND *POLYPTERUS PALMAS*

MARK W. WESTNEAT[1,*], MELINA E. HALE[1,2], MATTHEW J. McHENRY[3,4] AND JOHN H. LONG, Jr[3]

[1]*Department of Zoology, Field Museum of Natural History, Chicago, IL 60605-2496, USA,* [2]*Department of Organismal Biology and Anatomy, University of Chicago, Chicago, IL 60637, USA,* [3]*Department of Biology, Vassar College, Poughkeepsie, NY 12604, USA* and [4]*Department of Integrative Biology, University of California, Berkeley, CA 94720-3140, USA*

*e-mail: mwestneat@fmnh.org

Accepted 25 August; published on WWW 26 October 1998

Summary

The fast-start escape response is a rapid, powerful body motion used to generate high accelerations of the body in virtually all fishes. Although the neurobiology and behavior of the fast-start are often studied, the patterns of muscle activity and muscle force production during escape are less well understood. We studied the fast-starts of two basal actinopterygian fishes (*Amia calva* and *Polypterus palmas*) to investigate the functional morphology of the fast-start and the role of intramuscular pressure (IMP) in escape behavior. Our goals were to determine whether IMP increases during fast starts, to look for associations between muscle activity and elevated IMP, and to determine the functional role of IMP in the mechanics of the escape response. We simultaneously recorded the kinematics, muscle activity patterns and IMP of four *A. calva* and three *P. palmas* during the escape response. Both species generated high IMPs of up to 90 kPa (nearly 1 atmosphere) above ambient during the fast-start. The two species showed similar pressure magnitudes but had significantly different motor patterns and escape performance. Stage 1 of the fast-start was generated by simultaneous contraction of locomotor muscle on both sides of the body, although electromyogram amplitudes on the contralateral (convex) side of the fish were significantly lower than on the ipsilateral (concave) side. Simultaneous recordings of IMP, escape motion and muscle activity suggest that pressure change is caused by the contraction and radial swelling of cone-shaped myomeres. We develop a model of IMP production that incorporates myomere geometry, the concept of constant-volume muscular hydrostats, the relationship between fiber angle and muscle force, and the forces that muscle fibers produce. The timing profile of pressure change, behavior and muscle action indicates that elevated muscle pressure is a mechanism of stiffening the body and functions in force transmission during the escape response.

Key words: fast-start, Mauthner cell, fish, *Amia calva*, *Polypterus palmas*, locomotion, muscle pressure, myomere, electromyography, biomechanics.

Introduction

The fast-start escape response is a major predator avoidance behavior in fishes that involves rapid acceleration of the body away from a perceived threat. The typical fast-start is characterized by two initial stereotypic stages (Weihs, 1973). During stage 1, the fish bends laterally into a tight curve, rotating around its center of mass. The shape of the body at its maximum curvature has given this type of fast-start the name ‘C-start’. During stage 2, the fish takes its first propulsive tail stroke and accelerates away from the stimulus. Biologists have recognized the importance of this behavior to survival and have observed escape responses in many fish species across a broad phylogenetic diversity (e.g. Eaton *et al.* 1977; Fricke *et al.* 1987; Webb, 1978; Harper and Blake, 1990; Kasapi *et al.* 1993; Hale, 1996; Domenici and Blake, 1997). The fast-start provides an excellent model system for examining the interactions between neurobiology, muscle function and locomotor biomechanics in the production of a complex survival behavior.

The neurobiology and the behavior of fast-starts in fishes have received intensive study over the past two decades. Consequently, the neural circuitry and neuroanatomy that are the proximate causes of the fast-start are relatively well understood (Fetcho and Faber, 1988; Fetcho, 1990), as are the higher-level expressions of the behavior in terms of the kinematics of the body and the velocity of escape performance (for a review, see Domenici and Blake, 1997). How intervening levels of design such as muscle activity patterns, muscle force generation and transmission of forces through

tendons, skin and backbone interact to produce escape behavior is less well understood. We summarize below the mechanical system of the fast-start and develop a hypothesis for the role of axial muscle in transmitting forces for escape behavior. The experimental goal of this study is to test parts of this functional model of the fast-start.

Fast-starts are initiated by the Mauthner cells, the axons of which cross in the brain and extend posteriorly in the spinal cord on the opposite side of the body from the soma (Eaton *et al.* 1977; Zottoli, 1978). The circuitry of the startle response from Mauthner cells in the hind brain to interneurons and motoneurons posteriorly down the spinal cord has been mapped in several species (Fetcho and Faber, 1988; Fetcho, 1991). Firing of the Mauthner cell triggers the myomeres to contract simultaneously on the side of the body away from the stimulus and inhibits myomere contraction contralaterally (Fetcho and Faber, 1988; Eaton and Hackett, 1984). Thus, stimulation on one side of the body causes bending into a tightly curved position by differential effects on the left and right axial muscles.

Recent studies (Foreman and Eaton, 1993; Jayne and Lauder, 1993) have examined axial muscle activity during the escape response. Electromyogram (EMG) signals have been used to define the onset of stages 1 and 2 of the fast-start. Stage 1 begins with simultaneous ipsilateral muscle contraction, and the onset of stage 2 is defined as the beginning of contralateral muscle activity, which is nearly synchronous with a change in the direction of head motion (Foreman and Eaton, 1993). However, Jayne and Lauder (1993) showed that stage 1 EMG offset and stage 2 EMG onset are more variable than stage 1 activation. In addition, Foreman and Eaton (1993) showed that contralateral stage 2 EMG activity is absent in some responses. Muscle activity during escape has been recorded for few taxa, suggesting a critical need for EMG studies with simultaneous measurement of kinematics in a diversity of fishes.

Fast-start behavior and performance have been measured by computing the distance traveled, the directional change of the body and the velocity and acceleration of the body during escape (Domenici and Blake, 1997). Inter- and intraspecific variability is often high in these measures of fast-start behavior. Turning angles relative to initial orientation usually range between 0 and 180 ° to either side of the fish and are correlated with EMG duration (Eaton *et al.* 1981) and stimulus direction (Eaton and Emberley, 1991; Domenici and Batty, 1997). The velocity and acceleration performance of fast-starts vary across species (Webb, 1978; Domenici and Blake, 1997), and performance has been shown to be strongly affected by body size (Webb, 1976). Fast-start performance in early developmental stages is associated with the ontogeny of muscle structure (Hale, 1998), suggesting that the mechanical design of muscles for force transmission is a central determinant of fast-start behavior.

Muscle, connective tissue and the vertebral column produce and transmit force for fast-start behavior. However, the biomechanics of generating and transducing muscle forces through axial locomotor morphology is not well understood. The morphology of fish muscle has been described in order to determine the forces exerted by particular fiber angles in the myomere (Alexander, 1969; Videler, 1975), and biomechanical models have been proposed for the mechanism of force transduction through the complex structures of myomere, connective tissue and skin (Long and Nipper, 1996; Wainwright, 1983; Westneat *et al.* 1993). These studies have focused primarily on steady swimming rather than fast-starts, and broader comparative work focusing on the role of morphology and the mechanics of fast-starts in fishes has not been performed. In particular, the potential role of intramuscular pressure in the fast-start has not been explored.

When a muscle contracts, its internal pressure rises. This fact was documented in Hill's (1948) classic experiments on frog muscle, and the rise in internal pressure is used to measure the force produced by skeletal muscle (Ameredes and Provenzano, 1997; Ballard *et al.* 1992; Sejersted *et al.* 1984). However, few studies have measured intramuscular pressure (IMP) in non-mammalian vertebrates, investigated the mechanism of pressure generation in muscle or clarified the functional role of IMP in vertebrate musculoskeletal systems. The first such study in fishes (Wainwright *et al.* 1978) suggested that high IMP in sharks (20–200 kPa above ambient) puts the skin into tension, allowing it to act as an exotendon that transfers force to the tail for locomotor thrust. IMP has not been recorded from other fishes or from muscles contracting maximally. We hypothesize that IMP plays a central role in the fast-start of fishes because of the likelihood that elevated pressures are present during this forceful behavior with high body curvature.

Specifically, we propose the following mechanism for the generation and functional role of pressurized muscle in fast-start biomechanics. During a fast-start, the activated muscles shorten forcefully, causing the body to bend to that side. Associated with this shortening is a radial swelling of the muscle, a demonstrated characteristic of constant-volume muscular systems (Kier and Smith, 1985). Changes in body shape associated with radial swelling and axial bending are resisted globally by the cross-helical fibers of the skin (Wainwright *et al.* 1978) and regionally by the myosepta (Westneat *et al.* 1993), producing elevated intramuscular pressure. The functional role of IMP is to transmit forces to the skin and backbone by increasing the tension on the connective tissues of the myosepta. Muscle pressure, backbone stiffness and contralateral connective tissue stretching may resist stage 1 bending. In this case, IMP may store muscle work as elastic strain energy that is then used to help power the lateral tail sweep of the propulsive stage 2.

To test and refine these hypotheses of pressure generation and fast-start biomechanics, we have examined the relationships between intramuscular pressure, muscle activity patterns and escape behavior in *Polypterus palmas*, a bichir, and *Amia calva*, the bowfin. The timing and magnitude of pressure, EMG activity and kinematic variables provide the basis for a discussion of the muscular control of the fast-start in fishes and lead to the formulation of a general quantitative model of pressure generation in fish muscle. In addition, we

use these data to evaluate the locomotor function of elevated muscle pressure as a mechanism for stiffening the body and storing energy during the fast-start.

Materials and methods

Fishes

We studied the fast-start of *Polypterus palmas*, a bichir, and *Amia calva*, the bowfin. These species were chosen because (1) their phylogenetic positions are near the base of the major actinopterygian lineage of bony fishes and will provide important comparative data for evolutionary interpretation, (2) the flexible elasmoid scales and double-cone myomere of *A. calva* are functionally distinct from the heavy rhomboid armored scales and single-cone myomere of *P. palmas*, and (3) both fishes remain stationary and use the fast-start readily when stimulated. The data presented here for *A. calva* and *P. palmas* are part of an ongoing comparative study of fast-starts among basal actinopterygian fishes.

Amia calva were collected by seine and hook-and-line in the Big Muddy river in Southern Illinois. *Polypterus palmas* were purchased from aquarium dealers in Chicago. All fishes were maintained in 100 l aquaria at 20 °C. Sample sizes were three *P. palmas* (23.2–24.7 cm total length) and four *A. calva* (17.8–22.0 cm total length). Two fast-starts were analyzed for each fish, one response in which a cannula was implanted on the ipsilateral (concave) side and one response in which the cannula was implanted on the contralateral side, for a total of 14 fast-starts analyzed. This sample size was sufficient to examine overall patterns of pressure, EMG activity and kinematics and to make comparisons between species and between fast-start directions.

Intramuscular pressure

Intramuscular pressure was measured (Fig. 1) by surgically implanting a pressure cannula into the epaxial white muscle of the anesthetized fish. Fishes were anesthetized with tricaine methane sulfonate (MS222, Argent Chemicals), using approximately 0.5 g l^{-1} water. Anesthesia was usually complete within 5 min of immersion in the anesthetic. The oil-filled pressure cannula was implanted into the epaxial musculature slightly dorsal to the center of mass. The center of mass was determined by placing the fish on a balanced plastic tray with a fulcrum and adjusting the fish until the tray was balanced. The cannula was placed near the center of mass to minimize artifacts due to lateral acceleration during stage 1 of the fast-start. For *P. palmas*, a hole the size of the cannula (Intramedic polyethylene tubing, 1.1 mm i.d., 1.6 mm o.d.) was drilled into the middle of a ganoid scale. For *A. calva*, a small incision was made in the skin, through which the cannula was inserted. The cannula was inserted to a depth of 1.5 cm; the shaft of the cannula was then glued to the scale or skin using cyanoacrylic tissue cement and oriented perpendicular to the skin. The cannula was connected to a physiological pressure transducer (Gould/Statham, model T-P23ID) the output of which was amplified using a 40 kHz amplifier (Omega, model DMD-520). Pressure signals were recorded simultaneously on a high-speed video system (Kodak Systems 1000EM multi-channel data link) and a TEAC eight-channel (model RD-130TE) DAT tape recorder. Using this method, pressures were measured in units of force per unit area (in kN m^{-2}, or kPa). Pressure variables measured included the maximum pressure, the time to maximum pressure from the beginning of the fast-start and the duration of elevated pressure. Pressure duration was measured as the time between the beginning of fast-start motion and the point at which elevated pressure dropped to half-maximum pressure.

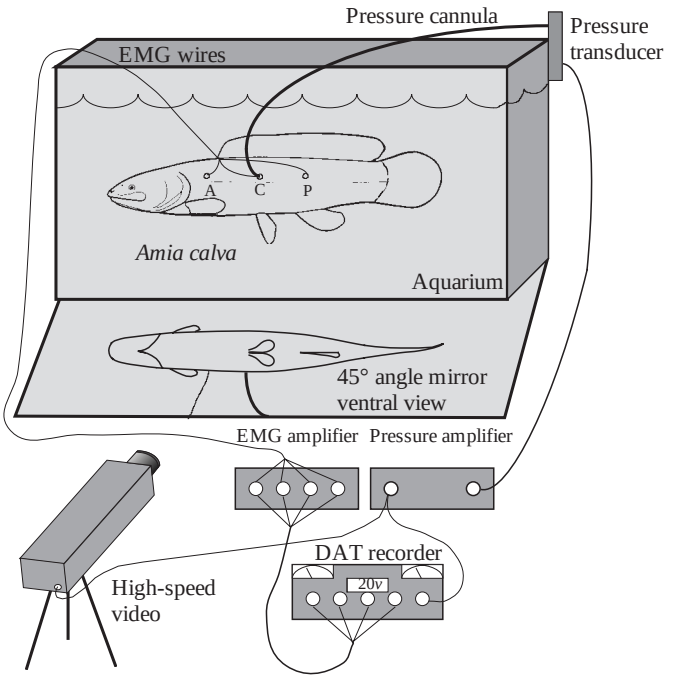

Fig. 1. Experimental apparatus for measuring fast-start behavior, electromyographic (EMG) activity in the axial muscles and intramuscular pressure. Video images in ventral view were recorded at 1000 Hz, EMG signals at 5000 Hz and intramuscular pressure profiles at 5000 Hz. A,P, anterior and posterior EMG recording sites; C, cannula site for measurement of intramuscular pressure. EMG electrodes were also implanted at site C and on the opposite midbody of the fish.

Electromyography

To measure muscle activity, fine-wire electrodes were implanted in four sites in the white epaxial musculature. Bipolar electrodes were constructed from 0.05 mm diameter, insulated, stainless-steel wire. Insulation was stripped from a 0.5 mm section of each wire to form an electrode tip with two bare wire sections 1.0 mm apart. Electrodes were threaded through a 25 gauge needle for implantation into muscles. Care was taken to standardize electrode construction to minimize signal variation. Electrodes were implanted at the cannula site (center of mass), 8–10 body segments anterior and posterior to the cannula site and on the opposite midbody of the fish. EMG signals were amplified by a factor of 5000–10 000 by AM

Systems (model 1700) amplifiers and recorded on a TEAC eight-channel (model RD-130TE) DAT tape recorder (Fig. 1). After the fish had been killed by immersion in an overdose of anesthetic (0.1 % solution MS-222), the electrodes were inspected by dissection to confirm their positions in the anterior-pointing cone of the myomere.

EMGs were later digitized using an NB-MIO-16 analog-to-digital converter driven by LabVIEW virtual instrument software (National Instruments Corp., Austin, TX, USA) at a sampling rate of 5000 point s^{-1} $channel^{-1}$. The digital record was then analyzed using a six-channel analysis algorithm custom-designed (M. Westneat) using the LabVIEW virtual instrument library. Analysis involved filtering the data with a high-pass Butterworth filter set at a sample rate of 5000 Hz and a low cut-off frequency of 60 Hz. Each channel was visually inspected to determine the baseline noise level; a cut-off amplitude was chosen, below which all values were set to zero. This allowed repeatable identification of the onset and offset of each muscle burst within an EMG recording. Only fast-starts with simultaneous muscle activation during stage 1 were selected for analysis.

The muscular motor pattern of each fast-start consisted of the measurement of 16 EMG variables of four types: (1) the duration (ms) of muscle activity; (2) the onset time (ms) of activity in other muscles relative to the time of first head motion; (3) the mean signal amplitude (mV) of each burst of activity; and (4) the area under the rectified (absolute value) EMG trace (in mV ms; computed by multiplying the mean signal amplitude of the rectified spikes by the duration of the burst).

Kinematics

After recovery, the fish were startled by a sudden movement and three electronic systems recorded data from the escape response (Fig. 1). A high-speed video camera recorded the motion of the fish at 1000 images s^{-1}, and intramuscular pressure was recorded simultaneously with EMG signals. Coordinates were taken from points digitized along the midline of the fish. The tip of the snout and the center of mass were digitized every 4 ms for *P. palmas* and every 2 ms for *A. calva*. Remaining midline points were digitized at equidistant intervals. Coordinate data were used to calculate the head velocity, the body velocity at the center of mass, the body curvature at the cannula site, the duration of stages 1 and 2, the distance traveled by the head during stage 1 and the distance traveled by the center of mass during stage 2. The fast-start began with first head motion detected. The end of stage 1 and beginning of stage 2 was defined as the point of reversal of direction of the head (usually near the point of maximal body curvature). Velocity and acceleration profiles were calculated using QuickSAND 5.0, a shareware program written by J. Walker for smoothing and numerical differentiation of time/distance data (Walker, 1998). Kinematic data included 17 midline points for *A. calva* and 20 midline points for *P. palmas*. To calculate curvature, a fifth-order polynomial equation was fitted to nine points, including the site of the pressure cannula and four points on either side. The first (y') and second (y'') derivatives of the polynomial equation were taken, and curvature (κ) was calculated at any point x using the following equation:

$$\kappa = \frac{|y''|}{(1 + y'^2)^{3/2}}. \quad (1)$$

Non-dimensional curvature was calculated by scaling κ (in m^{-1}) by body length (in m).

Control bending tests

To determine the role of simple bending of the body in the generation of intramuscular pressure, we bent the dead fish after an overdose of anesthetic. With the cannula intact, fish were manually bent with the cannula on the ipsilateral (concave) side and on the contralateral (convex) side. Electromyographic activity was absent during these tests, and pressure was recorded during bending through the range of curvatures observed during the fast-start.

Statistics

We used analyses of variance (ANOVAs) to test for significant differences in kinematic variables, pressure variables and motor patterns between species and between fast-starts in which the cannula was ipsilateral and contralateral. In addition to the main effects of species and fast-start direction (ipsilateral *versus* contralateral), we tested for a significant interaction between species and direction. To reduce the chances that significant differences would result from multiple tests on each data set, a strict Bonferroni correction was used to lower the probability level at which differences were judged significant: for kinematic variables (10 tests), $P<0.005$; for EMG activity (16 tests), $P<0.003$; for pressure profiles (three tests), $P<0.02$. All statistics were performed using JMP 3.0 (SAS Institute, Cary, NC, USA) on an Apple PowerMac G3 computer.

Morphology and modeling

Anatomical dissections were performed on fresh and preserved specimens of *Amia calva* and *Polypterus palmas* for the purpose of describing the morphology of the myomeres and the attachments of the myoseptal connective tissues to the backbone and skin (after Westneat *et al.* 1993). Myomeres near the center of mass were dissected to reveal their three-dimensional shape from a lateral view. Morphometric measurements were taken of the length and diameter of anterior-pointing cones. Three anterior-pointing cones were measured from three individuals of each species. Measurements were made using Helios dial calipers (precision 0.05 mm). Myomere geometry was used in a mechanical model of muscle cone function that estimates maximal intramuscular pressures. This model is based upon principles of cylindrical muscular hydrostats (Kier and Smith, 1985) and a previous model of muscle cone function (Westneat *et al.* 1993).

Results

The kinematics of the fast-start, the motor patterns of axial locomotor muscles that drive escape behavior and the pressure

profiles in locomotor muscle are described for two basal actinopterygian fishes, *Amia calva* and *Polypterus palmas*. Interspecific comparisons show that significant differences are present in performance measures, body curvature and motor patterns between the two species. The following sections detail the multiple data sets that are used to infer the mechanism of intramuscular pressure generation and the role of muscle pressure in escape behavior.

Fast-start mechanics in basal actinopterygians: species comparisons

During fast-start behavior (Fig. 2), *Amia calva* executed a classic C-start in which the body assumes a tight C-shape at the end of stage 1 (Fig. 2A, 40 ms). In stage 2, *A. calva* thrust the tail backwards to generate forward propulsion (Fig. 2A, 71 ms). *Polypterus palmas* performed an unusual fast-start in which the body was bent into an 'O' shape during stage 1 and the tip of the snout often contacted the tail (Fig. 2B, 158 ms). This fast-start shape is not a fundamentally different escape behavior, but rather is a C-start of an elongated fish in which the opening of the 'C' is closed. Escape performance of the fast-start was estimated by the distances traveled during stages 1 and 2 and the durations of stages 1 and 2, by head velocity and acceleration during stage 1 and by body velocity and acceleration at the center of mass (Table 1). The distance traveled did not differ between the two species. The durations of both stages of the fast-start of *A. calva* were significantly shorter than those of *P. palmas*: *A. calva* usually completed both stages of the behavior within 120 ms, whereas *P. palmas* fast-starts continued for nearly twice that long (Tables 1, 2; Figs 3–5). The two species had strikingly different velocity profiles, with *A. calva* showing a significantly greater head velocity (14.8 lengths s^{-1}) than *P. palmas* (9.1 lengths s^{-1}) and a significantly greater body velocity (7.5 lengths s^{-1}) than *P. palmas* (3.6 lengths s^{-1}). Non-dimensional curvature was significantly greater and was achieved significantly later in *P. palmas* than in *A. calva* (Tables 1, 2), with peak values for *P. palmas* ranging from 9.6 to 13.6, compared with 4.7 to 8.5 in *A. calva* (Table 1).

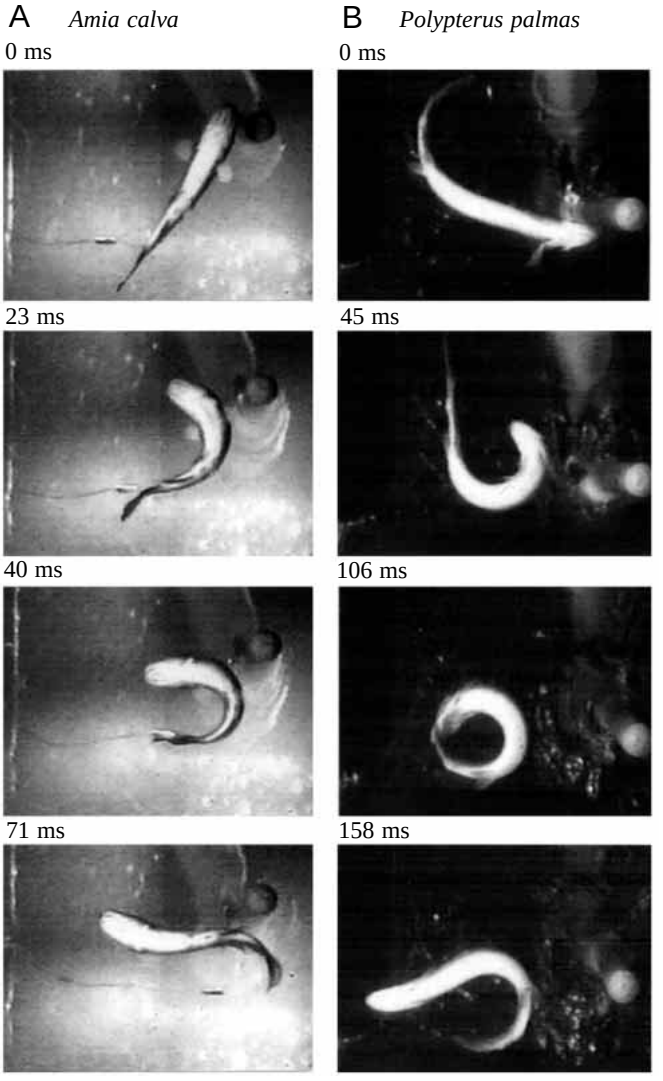

Fig. 2. Images from high-speed video recordings of (A) *Amia calva* and (B) *Polypterus palmas* fast-starts. The body accelerates from the resting position (first frames) through stage 1 (second frames) as the stimulus strikes next to the fish. Maximal curvature (third frames) is accompanied by peak pressures and is followed closely by stage 2 in which the tail is thrust backwards for maximal acceleration (last frames).

Stage 1 muscle activity in both species (Fig. 3) began simultaneously on both sides of the body and at all four electrode locations in response to the stimulus. In both species, curvature of the body and intramuscular pressure began to increase 5–10 ms after EMG onset. Curvature and pressure reached their peaks after stage 1 electrical activity in the muscles ceased (Figs 4, 5). Intramuscular pressure rose with increasing body curvature and increasing head velocity (Fig. 3). Pressure profiles were similar in the two species, with peak pressures ranging from approximately 20 kPa to 90 kPa, nearly 1 atmosphere above ambient (Table 1). *P. palmas* had a significantly longer elevated pressure duration and a significantly greater time to peak pressure (Table 2). Peak curvature and peak intramuscular pressure were not always simultaneous (e.g. note that peak pressure occurs after peak curvature for the *A. calva* data given in Fig. 4A).

Stage 2 muscle activity was strikingly different between *A. calva* and *P. palmas*. The *A. calva* profile of Fig. 3 shows a typical stage 2 pattern of muscle contraction for a contralateral fast-start, in which the three left-side electrodes detected stage 2 activity. This pattern consisted of the sequential onset of contraction from anterior to posterior as the propulsive stage of the fast-start was executed. In contrast to this pattern, there was rarely any muscular activity on the contralateral side in *P. palmas* and the typical pattern of sequential anterior–posterior contraction was never recorded. For example, Fig. 3 illustrates a representative contralateral fast-start of *P. palmas*, bending first away from the side with three electrodes, showing simultaneous Mauthner-cell-stimulated activity in all channels. In stage 2, when the fish reversed curvature and accelerated away from the stimulus, a small amount of activity was detected in the anterior electrode only. For the six fast-starts

Table 1. *Escape performance, escape timing, body curvature and intramuscular pressure variables for* Amia calva *and* Polypterus palmas

	Amia calva			*Polypterus palmas*		
	Range	Mean	S.D.	Range	Mean	S.D.
Stage 1 duration (ms)	32–47	38.4	5.6	75–103	90.8	10.5
Stage 2 duration (ms)	56–120	79.0	20.3	188–464	332.0	112.0
Distance traveled in stage 1 (*L*)	0.34–0.54	0.42	0.07	0.46–0.55	0.49	0.03
Distance traveled in stage 2 (*L*)	0.29–0.69	0.43	0.14	0.42–0.77	0.61	0.12
Maximum head velocity ($L\,s^{-1}$)	13.1–17.8	14.8	1.5	8.6–9.6	9.1	0.42
Maximum body velocity ($L\,s^{-1}$)	5.4–11.4	7.5	2.2	2.9–4.2	3.6	0.40
Maximum head acceleration ($L\,s^{-2}$)	237–1113	638	333	109–333	180	83
Maximum body acceleration ($L\,s^{-2}$)	90–533	294	148	75–147	117	31
Maximum curvature (dimensionless)	4.7–8.5	6.5	1.5	9.6–13.6	11.2	1.4
Time to maximum curvature (ms)	25–60	33.8	11.6	30–90	65.8	23.8
Maximum pressure (kPa)	19.6–90.1	45.8	22.6	13.8–85.9	33.7	26.7
Time to maximum pressure (ms)	29–89	45.1	20.9	25–130	77.7	33.7
Elevated pressure duration (ms)	75–140	109.4	20.3	90–210	150.8	38.3

Data include fast-starts in both directions (towards and away from the cannula).
For *Amia calva*, sample size is four individuals, eight fast-starts, for *Polypterus palmas*, *N*=3, 6.
L, total body length.
For statistical comparisons, see Table 2.

contained in the current data set, two responses showed low-level activity in a single electrode. Qualitative inspection of other fast-starts confirmed the lack of stage 2 activity in *P. palmas*.

The motor patterns of the two species were significantly different for all duration variables and all EMG integrated area variables (Tables 3, 4). EMG durations were significantly longer in *P. palmas* than in *A. calva* (Fig. 6A), although the onset times of muscle activity relative to the time of first head motion (Table 3; Figs 4, 5) were similar between the two species (Table 4). The mean signal amplitude of EMG bursts was similar across species, ranging from approximately 0.1 to approximately 1.0 mV. The integrated area of the EMG signal is the product of mean amplitude and duration, and this variable was significantly greater in *P. palmas* owing to the long durations of muscle contraction.

Stage 1 bending direction comparisons

We tested for differences in each of the kinematic, pressure and motor pattern variables between fast-start direction,

Table 2. *Results of ANOVA testing for significant differences between species and between ipsilateral and contralateral fast-starts for escape performance, escape timing, body curvature and intramuscular pressure changes for* Amia calva *and* Polypterus palmas

	Species		Direction		Species × Direction	
	F	*P*	*F*	*P*	*F*	*P*
Stage 1 duration	**126.32**	**<0.0001**	0.02	0.89	0.26	0.62
Stage 2 duration	**38.80**	**0.0001**	0.81	0.39	1.01	0.34
Distance traveled in stage 1	5.01	0.05	0.62	0.45	0.70	0.42
Distance traveled in stage 2	5.82	0.04	0.64	0.80	0.00	0.99
Maximum head velocity	**112.90**	**<0.0001**	2.96	0.11	2.21	0.16
Maximum body velocity	**19.17**	**0.001**	0.99	0.34	1.20	0.31
Maximum head acceleration	**23.6**	**0.0007**	9.4	0.01	5.0	0.05
Maximum body acceleration	7.5	0.02	0.26	0.62	0.63	0.45
Maximum curvature	**40.91**	**0.0001**	2.81	0.12	0.22	0.64
Time to maximum curvature	10.07	0.009	0.68	0.43	0.11	0.75
Maximum pressure	0.03	0.86	0.18	0.68	3.37	0.09
Time to maximum pressure	**9.96**	**0.01**	5.55	0.04	0.75	0.41
Elevated pressure duration	**126.31**	**<0.0001**	0.02	0.89	0.26	0.62

Values in bold type are significant.
Actual values are given in Table 1.

Table 3. *Electromyographic variables during stage 1 of the fast-start of* Amia calva *and* Polypterus palmas

	Amia calva			*Polypterus palmas*		
	Range	Mean	S.D.	Range	Mean	S.D.
Anterior EMG duration (ms)	27.8–76.2	38.2	15.8	67.2–98.2	82.1	11.2
Cannula EMG duration (ms)	29.2–51.0	35.4	6.9	67.2–93.6	85.7	9.7
Posterior EMG duration (ms)	28.4–52.4	35.6	7.6	78.0–101.4	86.9	7.9
Opposite EMG duration (ms)	22.0–47.4	35.0	8.4	66.8–90.2	76.9	9.9
Anterior EMG onset (ms)	−9.2 to −2.0	−5.5	3.1	−9.8 to −3.2	−6.5	2.8
Cannula EMG onset (ms)	−12.6 to −2.6	−7.0	3.3	−9.0 to −3.2	−5.9	2.4
Posterior EMG onset (ms)	−12.2 to −2.8	−6.8	3.3	−7.8 to −3.6	−5.6	1.7
Opposite EMG onset (ms)	−12.0 to −2.1	−6.0	3.4	−8.6 to −4.0	−6.1	1.9
Anterior EMG amplitude (mV)	0.09–1.07	0.61	0.35	0.51–1.02	0.73	0.18
Cannula EMG amplitude (mV)	0.19–1.06	0.70	0.35	0.43–1.50	0.86	0.38
Posterior EMG amplitude (mV)	0.25–1.03	0.71	0.31	0.41–0.98	0.70	0.22
Opposite EMG amplitude (mV)	0.14–1.05	0.66	0.34	0.33–0.91	0.69	0.23
Anterior EMG area (mV ms)	2.5–54.6	24.3	17.4	40.4–70.3	59.0	11.4
Cannula EMG area (mV ms)	5.7–45.7	25.2	13.9	40.3–129.4	73.6	34.2
Posterior EMG area (mV ms)	8.1–49.6	25.4	13.7	31.7–80.4	61.2	20.0
Opposite EMG area (mV ms)	4.8–44.2	22.6	13.0	23.3–80.0	54.8	19.9

Data includes fast-starts in both directions (towards and away from the cannula).
For *Amia calva*, sample size is four individuals, eight fast-starts; for *Polypterus palmas*, *N*=3, 6.
For statistical comparisons, see Table 4.

contrasting ipsilateral (towards the cannula) and contralateral (away from the cannula) responses (Tables 2, 4). Because we found that muscle was active on both sides of the fish simultaneously, the effects of direction for comparisons of EMG variables were of particular interest. We found no significant effect of fast-start direction for any of the kinematic or pressure variables nor for EMG duration (Fig. 6A) or relative onset features. Maximum body acceleration tended to be greater in *A. calva*, although this did not meet the Bonferroni-corrected significance level (Table 2). However, the mean signal amplitudes of the three left-side EMG channels were significantly greater during ipsilateral contractions than during contralateral fast-starts (Table 4; Fig. 6B). Similarly, the opposite side electrode showed greater amplitudes during

Table 4. *Results of ANOVA testing for significant differences between species and between ipsilateral and contralateral fast starts for electromyographic variables for* Amia calva *and* Polypterus palmas

	Species		Direction		Species × Direction	
	F	*P*	*F*	*P*	*F*	*P*
Anterior EMG duration	**36.6**	**0.0001**	0.02	0.89	3.10	0.11
Cannula EMG duration	**114.56**	**<0.0001**	0.06	0.46	0.01	0.93
Posterior EMG duration	**147.74**	**<0.0001**	1.75	0.22	0.07	0.80
Opposite EMG duration	**44.41**	**0.0001**	0.25	0.63	0.07	0.80
Anterior EMG onset	0.43	0.52	0.37	0.55	2.74	0.13
Cannula EMG onset	0.58	0.46	0.18	0.67	4.52	0.06
Posterior EMG onset	0.82	0.39	0.18	0.68	4.51	0.06
Opposite EMG onset	0.005	0.95	0.24	0.63	3.12	0.11
Anterior EMG amplitude	1.45	0.25	**15.48**	**0.003**	2.46	0.15
Cannula EMG amplitude	2.56	0.14	**37.75**	**0.0001**	0.02	0.89
Posterior EMG amplitude	0.003	0.95	**24.74**	**0.0006**	1.29	0.28
Opposite EMG amplitude	0.14	0.72	**34.60**	**0.0002**	1.69	0.22
Anterior EMG area	**31.68**	**0.0002**	7.86	0.02	2.06	0.18
Cannula EMG area	**48.57**	**<0.0001**	**31.35**	**0.0002**	5.14	0.05
Posterior EMG area	**47.83**	**<0.0001**	**26.18**	**0.0005**	0.94	0.35
Opposite EMG area	**35.86**	**0.0001**	**21.94**	**0.0009**	1.12	0.31

Values in bold type are significant.
Actual values are given in Table 3.

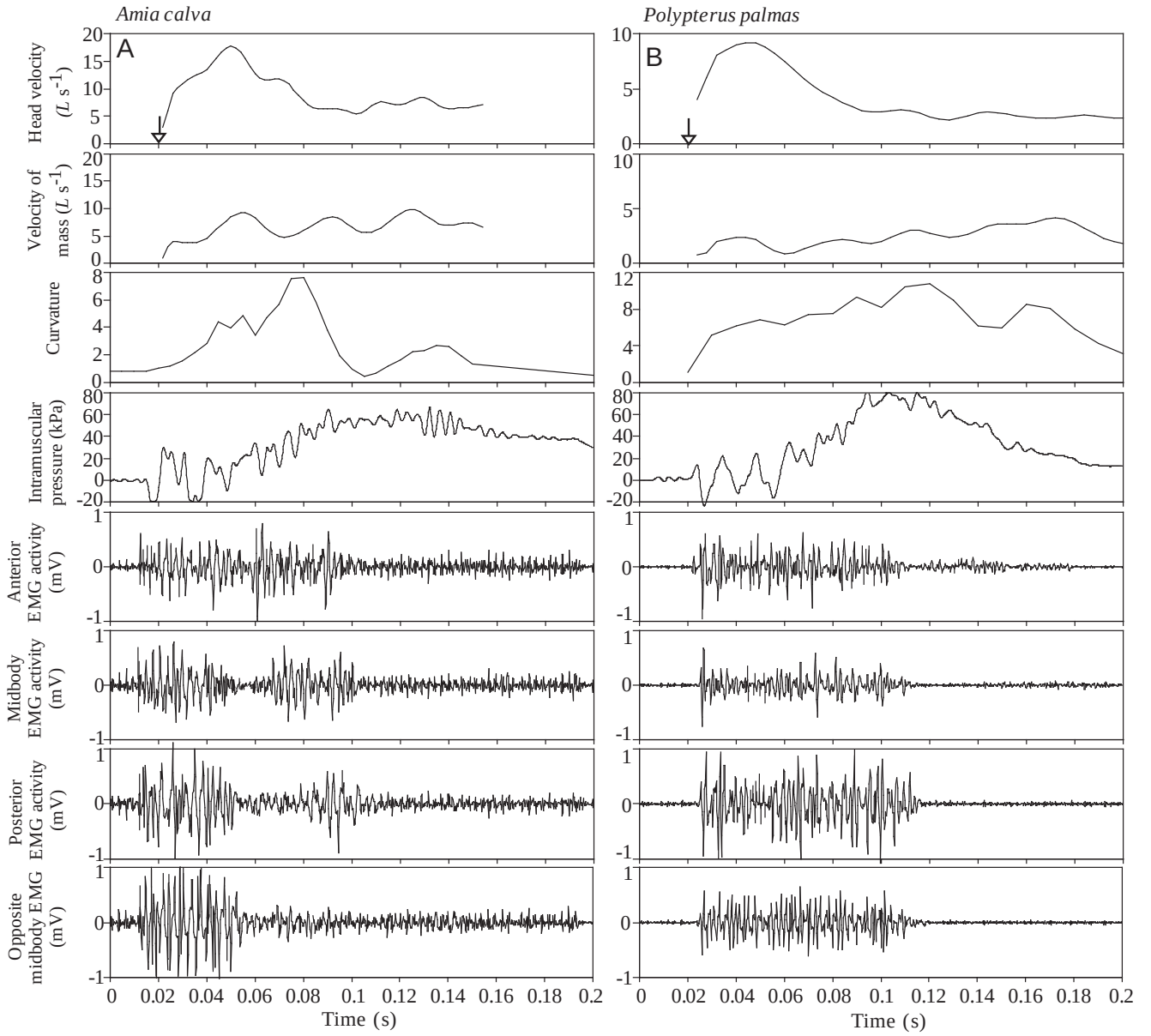

Fig. 3. Representative profiles of the fast-start of (A) *Amia calva* and (B) *Polypterus palmas*. Following the stimulus (arrow in top panels), the head is accelerated laterally to produce maximal body curvature. After peak curvature has been achieved, the escape velocity reaches its maximum. Intramuscular pressure oscillates initially as a result of vibration from the stimulus, then rises with increasing curvature and muscle activity. The four EMG channels fire simultaneously in a Mauthner-neuron-initiated fast-start. *L*, total body length. Curvature is non-dimensional.

contralateral fast-starts (Fig. 6B). The integrated areas of most EMG channels showed the same result, at lower significance levels. In other words, the strength of the EMG signals was always greatest on the side towards which the fish was bending.

Control bending

To examine the effect of body bending alone on muscle pressure, the intact, dead fish was manually bent at the end of the experiment (Fig. 7). Peak pressures during ipsilateral bends (towards the cannula) ranged from 10 to 15 kPa in *A. calva* and from 5 to 25 kPa in *P. palmas*. Contralateral bending caused pressure to fall below ambient to approximately −7 kPa in *A. calva* and to −5 to −20 kPa in *P. palmas*. This is in contrast to the pressure profiles during fast-starts which showed high, positive pressures during bending to both sides, with no significant difference between ipsilateral and contralateral sides.

Myomere morphology

A myomere is a set of muscle fibers that attaches anteriorly to one myoseptum and posteriorly to the next myoseptum. Muscle cells are generally oriented longitudinally, but their fiber angle with respect to the long axis of the fish varies with the position of the fiber in the section (Alexander, 1969). The

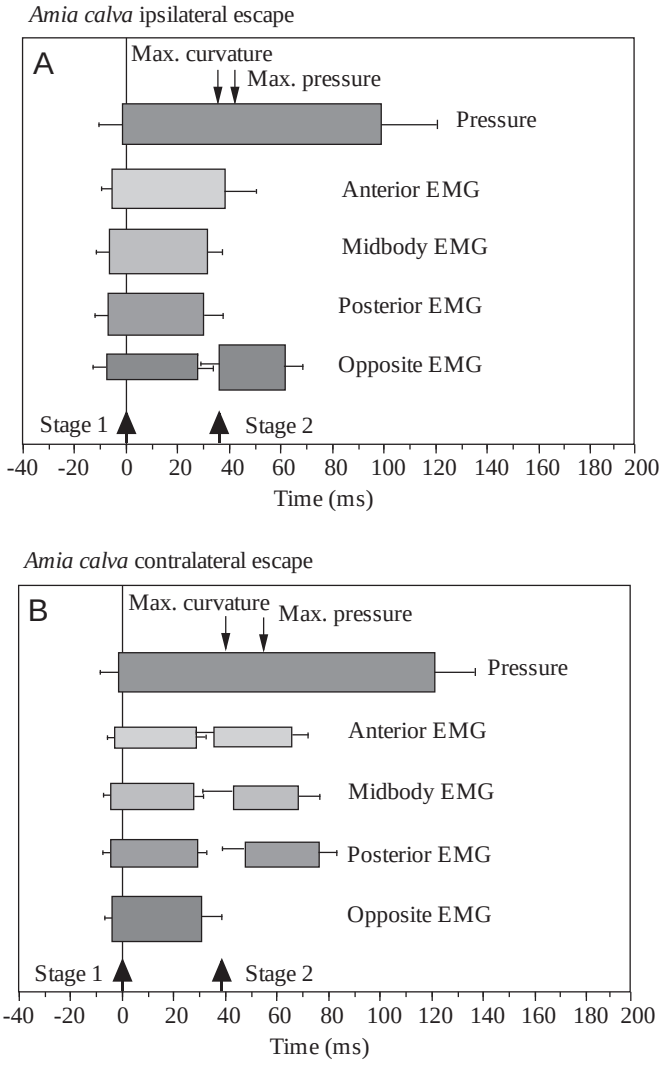

Fig. 4. Summary diagrams of the fast-start of *Amia calva*. Lengths of bars represent the mean duration of muscle activity or elevated pressure. Bar thickness indicates relative EMG amplitude. Error estimates at the start of each bar are the standard deviation in onset time relative to the first motion of the head (vertical line at time zero). Error estimates at the end of each bar are standard deviations of duration (N=4). (A) Ipsilateral fast-start; (B) contralateral fast-start.

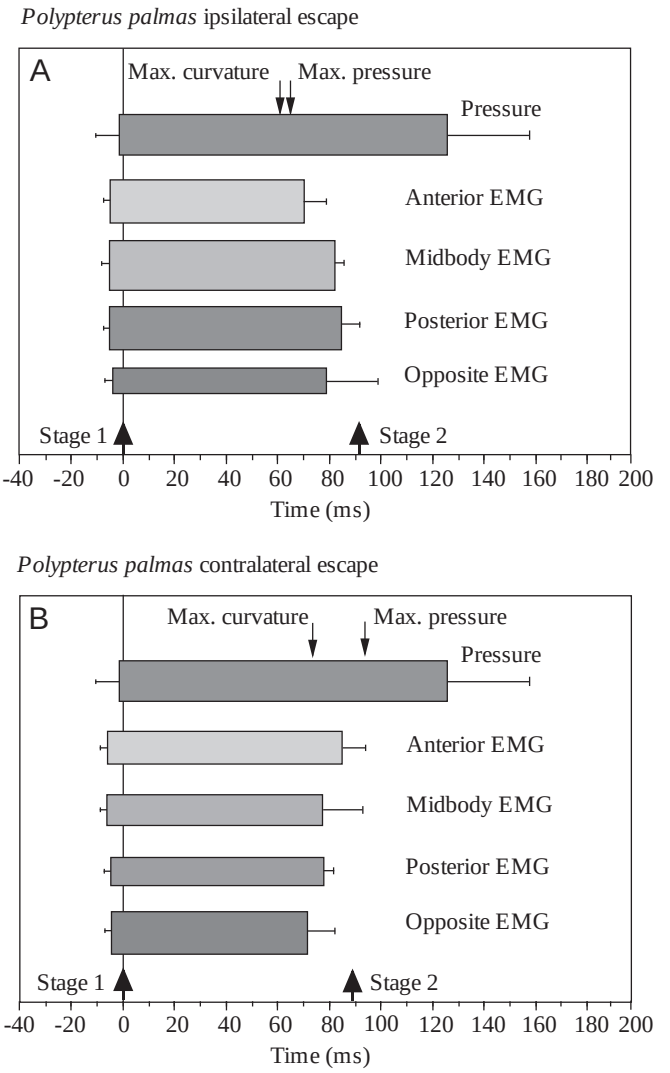

Fig. 5. Summary diagrams of the fast-start of *Polypterus palmas*. Lengths of bars represent the mean duration of muscle activity or elevated pressure. Bar thickness indicates relative EMG amplitude. Error estimates at the start of each bar are the standard deviation in onset time relative to the first motion of the head (vertical line at time zero). Error estimates at the end of each bar are standard deviations of duration (N=3). (A) Ipsilateral fast-start; (B) contralateral fast-start.

myosepta of *Polypterus palmas* and *Amia calva* have different three-dimensional structures (Fig. 8). Both species have anteriorly-directed cones of muscle that form the major muscle mass. These are the anterior-pointing cones (Fig. 8, APC). In *A. calva*, there are two APCs: one dorsal and one ventral to the main horizontal septum (Fig. 8B, MHS). In *P. palmas*, there is a single large APC that tapers sharply to a point (Fig. 8A). In both species, the myosepta have two small posterior-pointing cones (Fig. 8, PPC), one dorsal and one ventral to the APCs. The dorsalmost and ventralmost elements of the PPCs extend forwards as the anterior-pointing arms (Fig. 8, APA).

The myoseptum of the anterior-pointing cones is a fabric of crossed collagen fibers, with one tract of myoseptal fibers oriented generally longitudinally and another tract of fibers oriented circumferentially around the long axis of the APC. In both *A. calva* and *P. palmas*, these fibers attach medially to the vertebral column near the bases of the cones. Laterally, the longitudinal and circumferential tracts of fibers attach to the skin. In *P. palmas*, the myoseptal fibers attach prominently to the dermal collagen layer underlying the dermal scales.

The dimensions of the anterior-pointing cones were measured to develop a quantitative model for intramuscular pressure. For *A. calva*, the mean cone length was 7.95 mm and the mean diameter was 4.5 mm, whereas for *P. palmas*, the mean cone length was 13.5 mm and the mean diameter was 10.96 mm (Table 5).

Discussion

This study uses simultaneous, high-frequency acquisition of data on fast-start behavior, intramuscular pressure (IMP) profiles and the motor patterns of locomotor muscle to provide new insights into the biomechanics of the fast-start, a behavior central to the survival of almost all fishes. There are four central conclusions of this study. First, we demonstrate that *Amia calva* and *Polypterus palmas* generate high IMPs during the fast-start, often reaching nearly 1 atmosphere above ambient pressure. Second, our data on the timing of IMP and muscle activity support the hypothesis that the radial force of shortening myomeres is the mechanism of pressure generation. We propose a new model of IMP generation in fish muscle cones based on the anatomy of the myomeres of *A. calva* and *P. palmas*. Third, we show that central features of escape behavior, pressure profile and motor patterns are significantly different between the two species. The absence of stage 2 muscle contraction in *P. palmas* suggests that one functional role of elevated IMP is to provide force for the propulsive stroke of the fast-start. Finally, the myomeres on both sides of the fish contract strongly during a fast-start, although with different amplitudes and integrated areas. These data may help to refine models of Mauthner neuron function and suggest that myomeres function to stiffen the body during the fast-start.

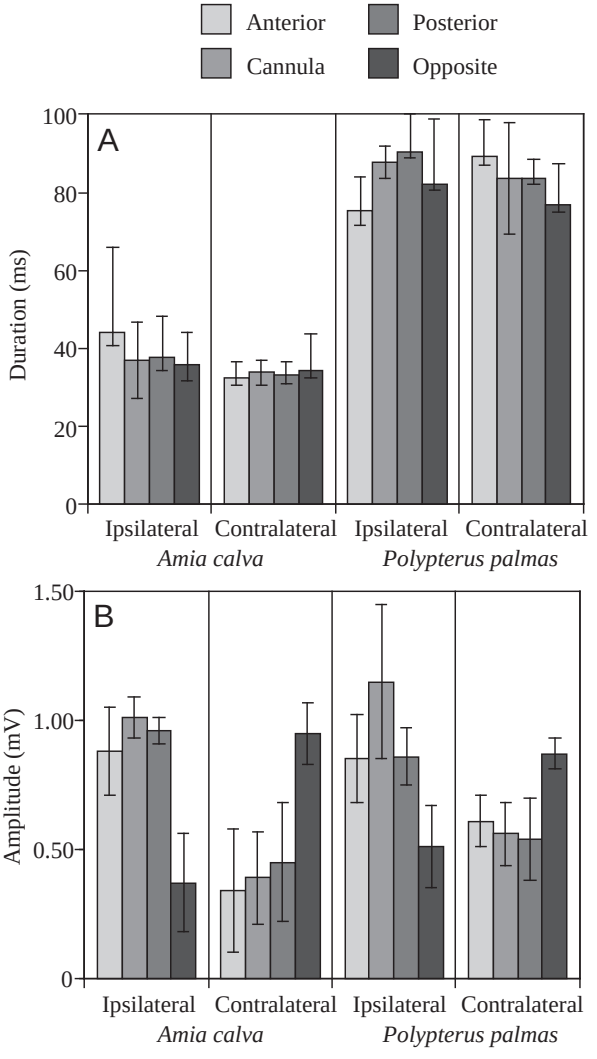

Fig. 6. (A) Duration of EMG bursts at the four electrode positions, showing significant differences between species, but similarity for the direction of the fast-start. (B) Amplitudes of EMG bursts at the four electrode positions, showing similarity between species, but significant differences for the direction of the fast-start. Values are means ± S.D. (for *A. calva*, *N*=4; for *P. palmas*, *N*=3).

Mechanics of pressure generation

A complete model of fast-start behavior, from neurobiology to behavior, requires an understanding of the generation and transmission of forces in axial tissues. Our results show that high intramuscular pressure is a primary aspect of force transmission during the fast-start. These data allow hypotheses regarding the causes and effects of elevated IMP to be refined. Recent models of the mechanical design of fish muscle (Wainwright, 1983; Westneat *et al.* 1993) have clarified how the generation of muscle forces depends on the three-dimensional morphology of the myomeres. The myomeres of *A. calva* and *P. palmas* (Fig. 8) are different in morphology, yet the basic cone-shaped structure of myomere segments suggests that similar mechanisms of pressure generation may be operating. *P. palmas* myomeres (Fig. 8A) have a single large median anterior-pointing cone, with a posteriorly directed cone dorsally and ventrally. In *A. calva*, a more typical teleostean myomere morphology is present, with two large central anterior-pointing cones (Fig. 8B). The myomeres are the source of the forces that drive escape behavior, and the distribution of those forces creates elevated IMP during locomotion.

There are two likely mechanisms of pressure generation during locomotion in fishes (Fig. 9). First, an increase in internal muscle pressure may be caused by the shortening and

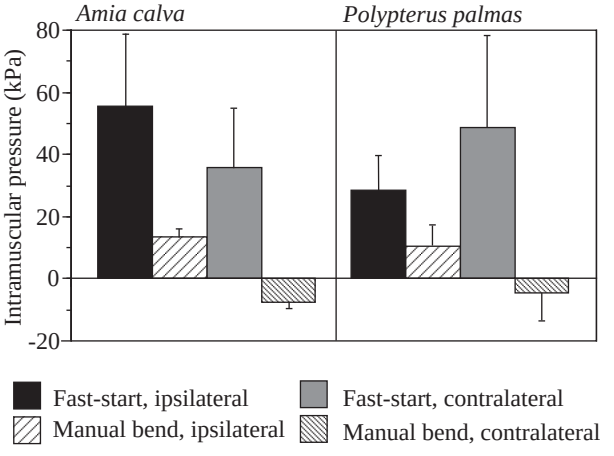

Fig. 7. Intramuscular pressure in *Amia calva* and *Polypterus palmas* during fast-start behavior and during manual bending of the anesthetized fish. Intramuscular pressures are significantly greater (*t*-test, $P<0.001$) during the fast-start, when muscle is active, than during manual bending of the inert fish. Values are means + S.D. (for *A. calva*, *N*=4; for *P. palmas*, *N*=3).

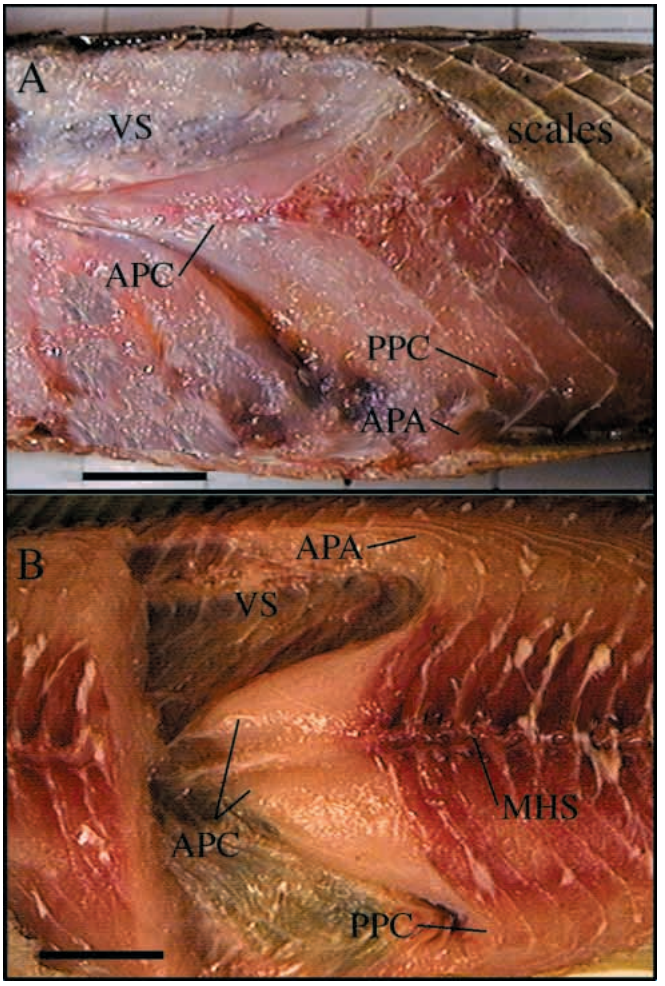

Fig. 8. Morphology of the myomeres of (A) *Polypterus palmas* and (B) *Amia calva*. The *P. palmas* myomere consists of a single large median anterior-pointing cone (APC), with a posteriorly directed cone (PPC) dorsally and ventrally and dorsal and ventral anterior-pointing arms (APA). The heavy ganoid scales wrap the muscle tightly with connective tissue, and groups of myoseptal fibers attach to the undersides of the ganoid scales. In *A. calva*, a more typical teleostean myomere morphology is present, with two large central anterior-pointing cones (APC), two posterior-pointing cones (PPC) and dorsal and ventral anterior-pointing arms (APA). VS, vertical septum; MHS, main horizontal septum. Scale bars, 1 cm.

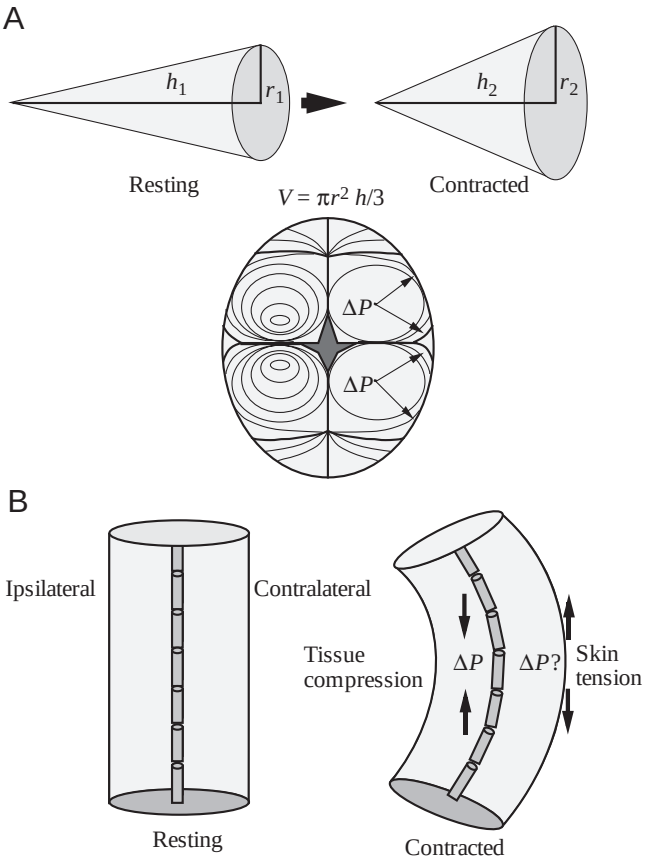

Fig. 9. Mechanical diagrams of two mechanisms of generation of intramuscular pressure. (A) Pressure change by contraction and radial expansion of muscle cones. A cone of height h and radius r_1 shortens, causing an increase in radius to r_2. The radial swelling of the cones (shown below in cross section) causes an increase in hydrostatic pressure (ΔP) in the space bounded by backbone, septa and skin because these structures resist the expansion. V, volume of the cone. (B) Pressure change by bending, causing a pressure increase (ΔP) on the ipsilateral and possibly the contralateral sides of the fish. As the cylindrical body bends, tissues are compressed on the ipsilateral side. Contralaterally, the skin is stretched in tension causing an increase in pressure in the muscle on the convex side of the body.

swelling of a constant volume of muscle tissue and by compression of the tissue against tendinous sheaths that surround the muscle (Fig. 9A). This model of force generation requires that muscle be actively contracting to produce locally elevated muscle pressure and has been proposed for bipennate muscles (van Leeuwen and Spoor, 1992) as well as for the cone-shaped muscle of tunas and mackerels (Westneat *et al.* 1993). In this model, IMP is the means by which the tendons that join the muscle, backbone and skin are put in tension to cause body bending. Pressures generated in this model depend upon the volume of muscle and the level of tension present in the connective tissues that surround the muscle.

In a second mechanism of pressure generation, pressure change is caused by lateral bending (Fig. 9B). In this model, bending puts tissues on the concave ipsilateral side of the body into compression, causing an increase in pressure. Tissues on the contralateral side of the body are put into tension. If skin tension compresses the muscle against the backbone and vertical septum, elevated intramuscular pressure would occur.

Our data from the fast-starts of *Amia calva* and *Polypterus palmas* indicate that the contraction and swelling of muscle, and not simple body curvature, cause the pressure change in fish muscle. During the fast-start, rising muscle pressure is associated with both EMG activity and increasing curvature (Fig. 3). However, in our control tests (Fig. 7) in which the anesthetized animals were manually forced into a physiological range of curvatures, small pressure increases

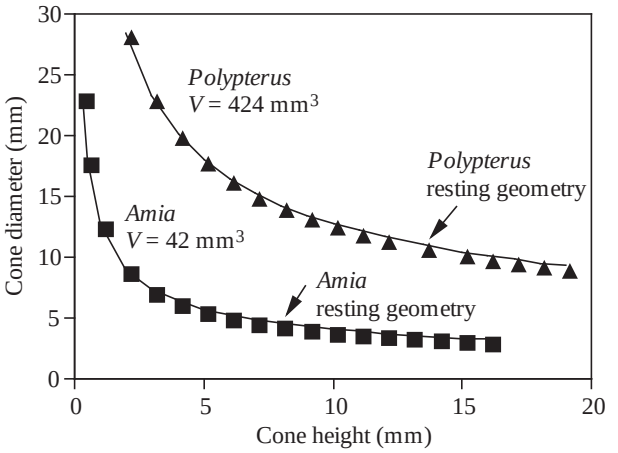

Fig. 10. The relationship between height and diameter for a cone of constant volume. Curves for the mean cone volumes (*V*) of *Amia calva* and *Polypterus palmas* are shown, with the resting dimensions of real myomeric cones indicated.

occurred on the ipsilateral side but pressure decreases were measured on the contralateral side. During the fast-starts of both species, elevated pressures were recorded when the cannula was on both the ipsilateral and contralateral sides. Furthermore, these pressure data agree with previous data on muscles in which bending did not occur: frog gastrocnemius muscle at pressures of 13–39 kPa (Hill, 1948), human vastus medialis muscle at 76 kPa (Sejersted *et al.* 1984) and canine gastrocnemius muscle at 70–200 kPa (Ameredes and Provenzano, 1997). In fishes, both muscle contraction and bending of the body affect internal pressure, although muscle contraction is of greater importance.

Modeling intramuscular pressure

The arrangement of serially homologous muscle segments in fishes into nested cones of muscle provides the basis for a more detailed model of IMP generation. Here, we propose a model of muscle contraction that incorporates myomere cone geometry, the concept of constant-volume muscular hydrostats, the relationship between fiber angle and muscle force, and previous physiological measurements of the forces that muscle fibers produce.

Muscular hydrostats will stiffen as they contract if they are wrapped with fibers that resist radial expansion (Kier and Smith, 1985; Wainwright *et al.* 1976). The mechanics of fiber-wound, pressurized cylinders depends upon the relationships between length, diameter, skin stress and wall thickness (Quillen, 1998). For a cylinder, circumferential stress (σ_{circ}) due to internal pressure is twice longitudinal skin stress (σ_{long}), $\sigma_{circ}=2\sigma_{long}$ (Wainwright *et al.* 1976). For a cone, the internal muscle pressure expanding laterally (the variable measured in this study) depends on total longitudinal muscle force, cone shape and cone volume because when the constant-volume longitudinal muscle cone contracts, it expands radially and increases the stress of the circumferential collagen fibers (Fig. 8; Westneat *et al.* 1993). We assume that internal muscle pressure is proportional to the degree of radial expansion of the cone.

Table 5. *Measurements of myomere anatomy and predicted changes in intramuscular pressure for* Amia calva *and* Polypterus palmas *using a quantitative model of myomere function based on muscle cone geometry*

	Amia calva		*Polypterus palmas*	
	Mean	s.d.	Mean	s.d.
Cone length (mm)*	7.95	0.21	13.5	0.50
Cone diameter (mm)	4.50	0.14	10.96	0.25
Cone volume (mm^3)	42.1	15.2	425.7	35.0
Cone surface area (mm^2)	74.2	5.3	251.1	14.5
Longitudinal force (N)	1.32	0.20	2.65	0.16
Radial force (N)	4.30	0.66	6.04	0.45
Pressure (kPa)	67.3	2.9	35.13	0.5
Force transmission advantage	3.27	0.13	2.28	0.03

Measured cone length is equivalent to cone height in the model. For *A. calva*, *N*=9; for *P. palmas*, *N*=9.

Thus, our model starts with the relationship between the height (h) and radius (r) of a cone-shaped, constant-volume muscular hydrostat (Figs 9A, 10). The volume of a cone is:

$$V = \frac{\pi r^2 h}{3}. \quad (2)$$

Cone volumes in *A. calva* and *P. palmas* differed by an order of magnitude as a result of the larger size of the single median cone of *P. palmas* (Table 5).

For a muscle cone of constant volume V, the relationship between the height and radius of the cone is:

$$r = \sqrt{\frac{3V}{\pi h}}. \quad (3)$$

This equation, when solved for a range of cone shapes (Fig. 10), reveals that changes in cone height, due to muscle contraction, translate into substantial radial expansion over a limited range of cone geometries. The resting geometries of the *A. calva* and *P. palmas* muscle cones are both positioned in the region of the curve where muscle shortening begins to be transmitted into increasing radial force, but before the exponentially increasing slope of radial expansion (Fig. 10).

To calculate longitudinal muscle force F_l, we use the equation of Calow and Alexander (1973) for a muscle whose fibers are at an angle to the primary direction of force:

$$F_l = \frac{V}{d}\delta\sin 2\alpha\ , \quad (4)$$

where V is volume, d is diameter, δ is muscle fiber force and α is muscle fiber angle to the long axis of the muscle. We used Altringham and Johnston's (1982) estimate of muscle fiber force per unit area in fish white muscle (200 $kN\,m^{-2}$) and Alexander's (1969) measurements of muscle fiber angles in the myomeres of *Amia calva* (20 °) and *Calamoichthys*, the sister

genus to *Polypterus* (15 °). Longitudinal muscle forces calculated using this equation for the average cones of *A. calva* and *P. palmas* were 1.3 and 2.7 N, respectively (Table 5).

In a cone-shaped muscular hydrostat, changes in longitudinal force are transmitted to radial force by the relationship between cone height and cone diameter shown in Fig. 10. Kier and Smith (1985) suggested that this mechanism in cylindrical muscular hydrostats is similar to that of a lever system, where the dimensions of the hydrostat determine lever mechanics. For a lever, the output force transmission (F_o) is equal to the product of input force (F_i) and inlever length (L_i) divided by outlever length (L_o). We propose that the transmission of force from longitudinal to radial is proportional to the change in cone dimensions during a muscle contraction. We calculated radial force F_r using the following equation:

$$F_r = F_l \frac{\Delta h}{\Delta d} , \quad (5)$$

Radial muscle forces for the average cones of *A. calva* and *P. palmas* were 4.3 and 6.0 N, respectively. These data illustrate that longitudinal shortening forces can be magnified by the properties of a fiber-wound, constant-volume hydrostatic muscle, similar to the properties of fiber-wound cylinders (Wainwright *et al.* 1976). The force transmission advantage ($\Delta h/\Delta d$) of *A. calva* was 3.3, whereas that of *P. palmas* was 2.3 (Table 5).

To compute pressure in kilopascals (kN m^{-2}), we divide radial force by the surface area A_s of the curved portion of the cone:

$$A_s = \pi r l \quad (6)$$

where

$$l = \sqrt{r^2 + h^2} . \quad (7)$$

Pressures calculated using the model for the average cones of *A. calva* and *P. palmas* were 67 and 35 kPa, respectively (Table 5). The proposed model thus estimates intramuscular pressures in the same range as observed during fast-start behavior. The model predictions are slightly greater than the means for both species (46 and 34 kPa, respectively), but fall well within the range of IMPs seen during escape behavior (Table 1).

A previous model of muscle architecture and IMP (van Leeuwen and Spoor, 1992) predicts a lower range of pressures (13–48 kPa) for bipennate muscles with a central tendon (typical of tetrapod limb muscles, for example). The computation of IMP in that model depends upon the tension and curvature of tendinous sheets and the angle and force of attached muscle fibers. The pressures estimated are thus localized and vary throughout a muscle. In contrast, our model is based upon the morphometrics of muscle shape for fish myomeres and estimates pressures that should be distributed across the surface of a muscle cone.

Various assumptions are made in this model, and it should be noted that alternative models may explain the data equally well. We model a cone-shaped muscular hydrostat that has a constant volume and resists radial expansion because of collagen fiber winding in its surface. We assume that the sequentially nested cones of adjacent myomeres act as a unit volume of muscle. This assumption is reasonable given that electromyographic studies of myomere activation have shown that regional areas of the body musculature in fishes are activated in concert (Jayne and Lauder, 1995). This model also ignores important issues of pressure distributions within a contracting muscle and the role of changing angles of muscle fibers and collagen fibers in complex muscle systems. Finally, our analysis does not clarify how the size and shape of muscular hydrostats may influence pressure magnitude and function, as Quillen (1998) demonstrated for hydrostatic skeletons. Further study of muscle pressure variation and myomere morphology will reveal the effects of cone geometry on IMP across taxa and help to refine mechanical models of pressurized vertebrate musculoskeletal systems.

Role of intramuscular pressure

Maximal elevated IMP occurs at a critical time in the escape response of fishes: at the transition from the preparatory stage 1 to the acceleratory stage 2 of a fast-start. Given that fishes generate intramuscular pressure during the fast-start, what is the functional role of this pressure change? One hypothesis (Wainwright *et al.* 1978) is that the skin is an exotendon that uses internal pressure as a means of active transfer of force to the caudal fin. This mechanism involves a helical winding of collagen fibers in the skin in which the fiber angle is greater than 55 ° to the longitudinal axis. Such a skin uses the force of internal pressure to transmit a longitudinal shortening posteriorly to the caudal region (Wainwright *et al.* 1978). This mechanism is likely to play a role in the mechanics of the fast-start, in which curvature peaks at the end of stage 1, followed by the rapid thrust of the posterior region of the body in stage 2. Recent simulations of fast-start mechanics (Ahlborn *et al.* 1997) show that propulsive forces in stage 2 depend upon a change in momentum of vortices associated with the tail fin. Increased force for the tail thrust of stage 2 will aid in achieving this reversal of momentum if the skin is in tension due to curvature and internal pressure.

A second possible role of IMP in the fast-start of fishes is to stiffen the body. If body stiffness increases, the natural oscillatory frequency increases, causing an increase in wave speed along the body (McHenry *et al.* 1995; Long *et al.* 1996). Experimental evidence for this principle was demonstrated by Long *et al.* (1996) in steady swimming in the long-nosed gar *Lepisosteus osseus*. Measurements of the dynamic flexural stiffness of intact and surgically altered gar skin showed that changes in the flexural stiffness of the skin altered the kinematics of undulatory locomotor waves in the body. Because wave speed in an oscillatory structure is proportional to the square root of the stiffness of the structure (Long, 1992), increased body stiffness due to increased IMP will probably increase the speed of undulatory wave propagation in stage 2 of the fast-start.

Intramuscular pressure may provide a mechanism for elastic recoil during stage 2 of the fast-start. Peak pressures occur at the end of stage 1, at which time the body is at maximal curvature. If internal pressure loads the skin in tension during a rapid increase in body curvature, this energy is available to accelerate the posterior body and caudal fin laterally without muscle activity during stage 2 of the fast-start. This mechanism is clearly playing a role in the fast-start of *P. palmas*, in which no stage 2 EMG bursts are seen on either side of the body (Figs 3B, 5). *P. palmas* appears to rely on body stiffness and the release of internal pressure and skin tension to uncoil the body during the propulsive stage of the escape. This is consistent with results showing that *P. palmas* uses elastic energy recoil during respiration (Brainerd, 1994).

The fast-start is a behavior of central importance to virtually all fishes that are subject to predation. Our results reveal a close association brtween elevated IMP, muscle activity and maximal body acceleration for the escape response. We suggest that the elevated internal muscle pressure transmits forces from the muscle to the skeletal system during the explosive fast-start response of fishes. Measurements of pressure along the body length and *in vivo* testing of skeletal deformation and skin tension are necessary to test this hypothesis.

Mechanism of the Mauthner response

Amia calva and *Polypterus palmas* showed strong stage 1 electromyographic signals on both sides of the body (Fig. 3) with no significant difference in the relative onset times of the EMG signal between the two sides (Tables 3, 4). Such simultaneous activation was not expected on the basis of models of the neural mechanism of the fast-start (Fetcho and Faber, 1988; Fetcho, 1990) in which contralateral muscle activity during stage 1 is inhibited.

Inhibition of the contralateral myomeres is evident in the EMG data presented here but with a more subtle effect than was expected. While contralateral myomere contraction is not prevented, it is weaker than on the side to which the fish is bending. For both species, the amplitude of the EMG signal is significantly lower on the contralateral side of the body (Table 4). Thus, the fish appears to bend in stage 1 not by preventing contralateral activity but by having a differential in the muscle force produced by the myomeres on the ipsilateral and contralateral sides of the body, with the greater force being produced on the side of the body to which the triggered Mauthner cell axon extends. The mechanism for partial inhibition is unclear.

The function of muscle contraction on both sides of the body is probably to increase stiffness in conjunction with muscle pressure. Long (1998) showed that when axial muscles are stimulated while they are lengthening, in eels, they serve simultaneously to increase stiffness up to three times the resting stiffness and to generate mechanical work to bend the body. In stage 1 of the fast-start, simultaneous activity of muscles on the contralateral side will thus increase stiffness and contribute to mechanical power for the stage 2 power stroke.

Stage 2 EMG signals differed significantly between *A. calva* and *P. palmas*. *A. calva* demonstrated a typical stage 2 signal of anterior to posterior muscle activation (e.g. Jayne and Lauder, 1993). *P. palmas*, in contrast, did not have stage 2 EMG bursts. The absence of stage 2 EMG bursts has been observed in other species (Foreman and Eaton, 1993), but such an activity pattern has been associated with the absence of a bend to the contralateral side of the body during stage 2 (Foreman and Eaton, 1993) or with the absence of stage 2 altogether (Domenici and Blake, 1997). The data for *P. palmas* differ in that there is a clear stage 2 body bend in the opposite direction to the stage 1 bend without coincident contralateral muscle activity.

In conclusion, a complete model of the mechanism of the fast-start requires the computation of muscle forces, the transmission of those forces to the backbone and skin, predictions of the rate and extent of body motion and, finally, estimates of locomotor thrust, hydrodynamics and escape speed. Such a complete model must await additional data on force production and the transmission properties of axial tissues, as well as information at other levels of design. We provide a model for the generation of muscle pressure during the fast-start and conclude that the function of muscle pressure is to store locomotor energy and to increase body stiffness. The contrasts between *Amia* and *Polypterus* suggest that the mechanics of pressurized axial muscle may be an important factor in the evolution of locomotor systems. Our finding that interspecific differences occur in behavior, performance, pressure profile and motor patterns indicates that substantial evolution has occurred in the biomechanics and neurobiology of this behavior. Our data for these two fishes at the base of actinopterygian phylogeny provide a basis for a broader study of fast-start behavior and motor control within the context of fish phylogeny.

We would like to express our deepest thanks to Steve Wainwright for his advice and interest in this project. His influence is clear all the way to the heart of this project, a fact that is reflective of the profound way in which he has fostered the careers of us all. Jeff Walker and his software QuickSAND were helpful in calculating velocity and accelerations. We thank Bill Browne and Tom Anton for their assistance with field work in capturing *Amia calva*. This research was supported by NSF grant IBN-9407253 to M.W.W., ONR grant N00014097-1-0292 to J.H.L., NSF Dissertation Grant IBN 9423525 to M.E.H. and a Predoctoral Fellowship to M.E.H. from the Howard Hughes Medical Institute.

References

AHLBORN, B., CHAPMAN, S., STAFFORD, R., BLAKE, R.W. AND HARPER, D. G. (1997). Experimental simulation of the thrust phases of fast-start swimming of fish. *J. exp. Biol.* **200**, 2301–2312.

ALEXANDER, R. MCN. (1969). The orientation of muscle fibers in the myomeres of fishes. *J. mar. biol. Ass. U.K.* **49**, 263–290.

ALTRINGHAM, J. D. AND JOHNSTON, I. A. (1982). The pCa–tension and force–velocity characteristics of skinned fibers isolated from fish fast and slow muscles. *J. Physiol., Lond.* **333**, 421–449.

AMEREDES, B. T. AND PROVENZANO, M. A. (1997). Regional

intramuscular pressure development and fatigue in the canine gastrocnemius muscle *in situ*. *J. appl. Physiol*. **83**, 1867–1876.

BALLARD, R. E., ARATOW, M., CRENSHAW, A., STYF, J., KAHAN, N., WATENPAUGH, D. E. AND HARGENS, A. R. (1992). Intramuscular pressure measurement as an index of torque during dynamic exercise. *Physiologist* **35**, 115–116.

BRAINERD, E. L. (1994). Mechanical design of polypterid fish integument for energy storage during recoil aspiration. *J. Zool., Lond*. **232**, 7–19.

CALOW, L. J. AND ALEXANDER, R. MCN. (1973). A mechanical analysis of a hind leg of a frog (*Rana temporaria*). *J. Zool., Lond*. **171**, 293–321.

DOMENICI, P. AND BATTY, R. S. (1997). Escape manoeuvres of schooling *Clupea harengus*. *J. Fish Biol*. **45** (Suppl. A), 97–110.

DOMENICI, P. AND BLAKE, R. W. (1997). The kinematics and performance of fish fast-start swimming. *J. exp. Biol.* **200**, 1165–1178.

EATON, R. C., BOMBARDIERI, R. A. AND MEYER, D. H. (1977). The Mauthner initiated startle response in teleost fish. *J. exp. Biol.* **66**, 65–81.

EATON, R. C. AND EMBERLEY, D. S. (1991). How stimulus direction determines the trajectory of the Mauthner-initiated escape response in teleost fish. *J. exp. Biol.* **161**, 469–487.

EATON, R. C. AND HACKETT, J. T. (1984). The role of the Mauthner cell in fast-starts involving escape in teleost fishes. In *Neural Mechanisms of Startle Behavior* (ed. R. C. Eaton), pp. 213–266. New York: Plenum Press.

EATON, R. C., LAVENDER, W. A. AND WIELAND, C. M. (1981). Identification of Mauthner-initiated response patterns in goldfish: evidence from simultaneous cinematography and electrophysiology. *J. comp. Physiol.* **144**, 521–531.

FETCHO, J. R. (1990). Morphological variability, segmental relationships and functional roles of a class of commissural interneurons in the spinal cord of goldfish. *J. comp. Neurol.* **299**, 283–298.

FETCHO, J. R. (1991). Spinal network of the Mauthner cell. *Brain Behav. Evol*. **37**, 298–316.

FETCHO, J. R. AND FABER, D. S. (1988). Identification of motoneurons and interneurons in the spinal network for escapes initiated by the Mauthner cell in goldfish. *J. Neurosci.* **8**, 4192–4213.

FOREMAN, M. B. AND EATON, R. C. (1993). The direction change concept for reticulospinal control of goldfish escape. *J. Neurosci.* **13**, 4101–4133.

FRICKE, H., REINICKE, O., HOFER, H. AND NACHIGALL, W. (1987). Locomotion of the Coelacanth *Latimeria chalumnae* in its natural environment. *Nature* **329**, 331–333.

HALE, M. E. (1996). The development of fast-start performance in fishes: Escape kinematics of the chinook salmon (*Oncorhynchus tshawytscha*). *Am. Zool*. **36**, 695–709.

HALE, M. E. (1998). Developmental and evolutionary biomechanics of the fast-start escape response in fishes. PhD dissertation, University of Chicago. 261pp.

HARPER, D. G. AND BLAKE, R. W. (1990). Fast-start performance of rainbow trout *Salmo gairdneri* and northern pike *Esox lucius*. *J. exp. Biol*. **150**, 321–342.

HILL, A. V. (1948). The pressure developed in muscle during contraction. *J. Physiol., Lond.* **107**, 518–526.

JAYNE, B. C. AND LAUDER, G. V. (1993). Red and white muscle activity and kinematics of the escape response of bluegill sunfish during swimming. *J. comp. Physiol.* A **173**, 495–508.

JAYNE, B. C. AND LAUDER, G. V. (1995). Are muscle fibers within fish myotomes activated synchronously? Patterns of recruitment within deep myomeric musculature during swimming in largemouth bass. *J. exp. Biol.* **198**, 805–815.

KASAPI, M. A., DOMENICI, P., BLAKE, R. W. AND HARPER, D. G. (1993). The kinematics and performance of the escape response in the knifefish *Xenomystus nigri*. *Can. J. Zool*. **71**, 189–195.

KIER, W. M. AND SMITH, K. K. (1985). Tongues, tentacles and trunks: the biomechanics of movement in muscular hydrostats. *Zool. J. Linn. Soc*. **83**, 307–324.

LONG, J. H., JR (1992). Stiffness and damping forces in the intervertebral joints of the blue marlin (*Makaira nigricans*). *J. exp. Biol.* **162**, 131–155.

LONG, J. H., JR (1998). Muscles, elastic energy and the dynamics of body stiffness in swimming eels. *Am. Zool.* (in press).

LONG, J. H., JR, HALE, M. E., MCHENRY, M. J. AND WESTNEAT, M. W. (1996). Functions of fish skin: the mechanics of steady swimming in longnose gar *Lepisosteus osseus*. *J. exp. Biol.* **199**, 2139–2151.

LONG, J. H., JR AND NIPPER, K. S. (1996). The importance of body stiffness in undulatory propulsion. *Am. Zool*. **36**, 678–694.

MCHENRY, M. J., PELL, C. A. AND LONG, J. H., JR (1995). Mechanical control of swimming speed: stiffness and axial wave form in undulating fish models. *J. exp. Biol.* **198**, 2293–2305.

QUILLEN, K. J. (1998). Ontogenetic scaling of hydrostatic skeletons: geometric, static stress and dynamic stress scaling of the earthworm *Lumbricus terrestris*. *J. exp. Biol.* **201**, 1859–1870.

SEJERSTED, O. M., HARGENS, A. R., KARDEL, K. R., BLOM, P., JENSEN, O. AND HERMANSEN, L. (1984). Intramuscular fluid pressure during isometric contraction of human skeletal muscle. *J. appl. Physiol*. **56**, 287–295.

VAN LEEUWEN, J. L. AND SPOOR, C. W. (1992). Modelling mechanically stable muscle architectures. *Phil. Trans. R. Soc. Lond B* **336**, 275–292.

VIDELER, J. J. (1975). On the interrelationships between morphology and movement in the tail of the cichlid fish *Tilapia nilotica*. *Neth. J. Zool*. **25**, 144–194.

WAINWRIGHT, S. A. (1983). To bend a fish. In *Fish Biomechanics* (ed. P. Webb and D. Weihs), pp. 68–91. New York: Praeger Press.

WAINWRIGHT, S. A., BIGGS, W. D., CURREY, J. D. AND GOSLINE, J. M. (1976). *Mechanical Design in Organisms*. New York: John Wiley & Sons. 423pp.

WAINWRIGHT, S. A., VOSBURGH, F. AND HEBRANK, J. H. (1978). Shark skin: function in locomotion. *Science* **202**, 747–749.

WALKER, J. A. (1998). Estimating velocities and accelerations of animal locomotion: a simulation experiment comparing numerical differentiation algorithms. *J. exp. Biol.* **201**, 981–995.

WEBB, P. W. (1976). The effect of size on the fast-start performance of rainbow trout *Salmo gairdneri* and a consideration of piscivorous predator–prey interactions. *J. exp. Biol.* **65**, 157–177.

WEBB, P. W. (1978). Fast-start performance and body form in seven species of teleost fish. *J. exp. Biol.* **74**, 211–226.

WEIHS, D. (1973). The mechanism of rapid starting of slender fish. *Biorheology* **10**, 343–350.

WESTNEAT, M. W., HOESE, W., PELL, C. A. AND WAINWRIGHT, S. A. (1993). The horizontal septum: mechanisms of force transfer in locomotion of scombrid fishes (Scombridae, Perciformes). *J. Morph*. **217**, 183–204.

ZOTTOLI, S. J. (1978). Comparative morphology of the Mauthner-cell in fish and amphibians. In *Neurobiology of the Mauthner Cell* (ed. D. S. Faber and H. Korn), pp. 13–45. New York: Raven Press.